Dynamics of vortex-antivortex pairs and rarefaction pulses in liquid light

David Feijoo, Angel Paredes, and Humberto Michinel
Departamento de Física Aplicada, Universidade de Vigo, As Lagoas s/n, Ourense ES-32004, Spain
(Received 1 December 2016; published 9 March 2017)

We present a numerical study of the cubic-quintic nonlinear Schrödinger equation in two transverse dimensions, relevant for the propagation of light in certain exotic media. A well-known feature of the model is the existence of flat-top bright solitons of fixed intensity, whose dynamics resembles the physics of a liquid. They support traveling wave solutions, consisting of rarefaction pulses and vortex-antivortex pairs. In this work, we demonstrate how the vortex-antivortex pairs can be generated in bright soliton collisions displaying destructive interference followed by a snake instability. We then discuss the collisional dynamics of the dark excitations for different initial conditions. We describe a number of distinct phenomena including vortex exchange modes, quasielastic flyby scattering, solitonlike crossing, fully inelastic collisions, and rarefaction pulse merging.

DOI: 10.1103/PhysRevE.95.032208

I. INTRODUCTION

The synergy between competing nonlinearities in the Schrödinger equation can give rise to very interesting dynamics [1,2], including, for instance, solitons [3,4] and phase transitions [5,6]. In this paper, we provide insights on the cubic-quintic (focusing-defocusing) model, which has been thoroughly studied in the context of nonlinear optics [7–9], where it was shown that large power solitons have neat similarities with regular liquids, thereby motivating the term "liquid light" [10]. The same equation has been applied in other frameworks too, see, e.g,, Refs. [11–15].

The cubic-quintic equation is an appropriate model for the propagation of light in certain optical materials, see for instance Ref. [16] and references in Ref. [17]. It has also been used as an approximation to the process of filamentation [18–20]. Recent experimental advances reinforce the significance of new theoretical studies. Despite damping, (limited) soliton propagation has been observed in carbon disulfide [21]. Furthermore, the dropletlike behavior of cubic-quintic propagation has been demonstrated in atomic gases at low optical powers [22,23], using quantum coherence and interference as proposed in Refs. [24,25]. Other setups in which the fifth-order nonlinearity can be enhanced through quantum effects comprise Rydberg atoms [26] and quantum dots [27,28]. Confinement and guiding of light in a cubic-quintic (defocusing-focusing) has also been reported [29].

In the cubic-quintic model, there is a one-parameter family of form-preserving traveling dark wave solutions within a critical bright background, which was computed in Ref. [30] following the numerical methods of Ref. [31]. For small velocities, it consists of vortex-antivortex pairs of charges ± 1 (we will make a usual abuse of language and refer to "velocity" for what in the optical setup corresponds to the propagation angle with respect to the axis). For larger subsonic velocities, the solutions are rarefaction pulses, namely dark blobs without vorticity. The fainter the pulse is, the faster it moves within the bright background. This family of solutions is similar to the one existing for third-order defocusing nonlinearity [32–35]. Rarefaction pulses should not be confused with the unstable quiescent bubbles of [36,37].

A separate issue is how these dark solitonlike excitations can be generated dynamically. In the context of Bose-Einstein condensates (BECs), they have been generated by phase imprinting [38]. In the framework of superfluids, it was shown that they can appear when the fluid flows past an obstacle [39], a process that in optics can be mimicked by the nonlinear interaction with an incoherently coupled beam [40] and in BECs with a laser beam (see Ref. [41] and references therein).

A remarkable result of Ref. [30] is that, for the liquid of light, rarefaction pulses can be generated by interference in the collision of two bright solitons of very different sizes and powers. The analogy with bubbles in fluids motivates the usage of the term "cavitation" for this kind of process. The produced caviton excitation propagates within the large soliton and can exit it becoming a bright soliton again. This bright-dark-bright conversion is familiar in one dimension, see, e.g., Refs. [42,43], but it is a distinctive feature of the cubic-quintic equation in two dimensions. This peculiarity facilitates the creation of dark traveling waves in a controlled manner from initial conditions comprising only bright solitons. With three initial bright solitons, two separate traveling waves can be created within the same fluid.

The natural question that we address in the present paper is how these traveling waves interact with each other. It would be really interesting to implement this kind of processes in experimental setups as those described in Refs. [21–23]. For the case of defocusing cubic nonlinearity, the dynamics of the dark excitations in a nontrivial background was analyzed in Refs. [44–46] and their interaction with a single vortex in Ref. [47].

In Sec. II, we fix notation and review some features of the cubic-quintic model. In Sec. III, we show that vortex-antivortex pairs can be produced by a soliton-soliton collision. Sections IV–VI describe the result of our simulations concerning dark wave interactions. We discuss in turn the collision of two vortex-antivortex pairs, that of a rarefaction pulse with a vortex-antivortex and that of two rarefaction pulses. In Sec. VII we outline our conclusions and make some final remarks. The Supplemental Material [48] contains animations for all of the examples of dynamical evolution that are presented along the paper and a few extra illustrative cases.

II. SOLITONS AND TRAVELING WAVES

In this section we briefly review well-known results concerning the cubic-quintic model in order to provide the

basic ingredients for the following. Consider the paraxial propagation of a laser beam of angular frequency $\omega = k_0 c$ in a medium with refractive index $n = n_0 + \Delta n$:

$$-2ik_0 n_0 \frac{\partial A}{\partial \hat{z}} = \left(\partial_{\hat{x}}^2 + \partial_{\hat{y}}^2\right) A + 2\Delta n k_0^2 n_0 A, \tag{1}$$

where n_0 is a constant and terms of order $\mathcal{O}(\Delta n^2)$ have been neglected. We use $\hat{x}$, $\hat{y}$, $\hat{z}$ for dimensionful coordinates. The intensity is given by $I = \frac{n_0}{2}\sqrt{\frac{\epsilon_0}{\mu_0}}|A|^2$. We assume the following nonlinear correction to the refractive index $\Delta n = n_2 I + n_4 I^2$ with $n_2 > 0$, $n_4 < 0$. It is convenient to rescale Eq. (1) to dimensionless quantities:

$$A = \left(-\frac{2n_2}{n_0 n_4}\sqrt{\frac{\mu_0}{\epsilon_0}}\right)^{\frac{1}{2}} \psi, \quad \hat{z} = -\frac{n_4}{k_0 n_2^2} z,$$
$$(\hat{x}, \hat{y}) = \frac{1}{k_0 n_2}\sqrt{\frac{-n_4}{2n_0}}(x, y). \tag{2}$$

The power of the beam is given by $\hat{P} = \int I d\hat{x} d\hat{y} = (2k_0^2 n_0 n_2)^{-1} P$ where the dimensionless power is $P = \int |\psi|^2 dx dy$.

With the transformation (2), we find the canonical equation governing the wave amplitude $\psi(x, y, z)$:

$$i\partial_z \psi = -\left(\partial_x^2 + \partial_y^2\right)\psi - (|\psi|^2 - |\psi|^4)\psi. \tag{3}$$

The translation from dimensionless to physical quantities depends on the particular system. Below, we will just deal with Eq. (3), but it is interesting to provide the transformation for a benchmark example. Consider the case of Ref. [21] where $n_0 = 1.6$, $n_2 = 3.1\times10^{-19}\mathrm{m}^2/\mathrm{W}$, $n_4 = -5.2\times10^{-35}\mathrm{m}^4/\mathrm{W}$, $\lambda = 2\pi/k_0 = 920\times10^{-9}\mathrm{m}$. Then, the unit of z corresponds to 79 μm, the unit of x or y to 1.9 μm and the unit of power to 21.6 kW. Notice that in the setup [21] there is a nonlinear absorption term that has not been included here.

There are stable solitary wave solutions of Eq. (3) of the form $\psi = e^{i\beta z} f(r)$ with $\lim_{r\to\infty} f(r) = 0$, which we laxly call bright solitons, as it is customary in the literature. The numerical study of Refs. [9,10] shows that there are solutions for $0 < \beta < \beta_{cr} = \frac{3}{16}$. The power $P = 2\pi \int r f(r)^2 dr$ grows monotonically with β in the range $P_0 < P < \infty$ where P_0 is the minimal value that leads to self-trapping. For small β, the function $f(r)$ is bell shaped. Near the β_{cr} eigenvalue cutoff [49], $f(r)$ tends to a flat-top profile. This means that $f \approx \Psi_{cr} = \frac{\sqrt{3}}{2}$ for $r < r_{\mathrm{sol}}$ and around the soliton radius r_{sol} there is a quick drop to $f \approx 0$ for $r > r_{\mathrm{sol}}$. This limit is the liquidlike phase, in which the soliton resembles a fluid with constant density and fixed surface tension subject to the Young-Laplace equation [50].

We will use these bright solitons to define the initial conditions of simulations in the following sections, by considering

$$\psi|_{z=0} = f_1(|\mathbf{x}|) + f_2(|\mathbf{x} - \mathbf{x_2}|)\exp\left(i\frac{\mathbf{v_2}\cdot\mathbf{x}}{2} + i\phi_2\right)$$
$$+ f_3(|\mathbf{x} - \mathbf{x_3}|)\exp\left(i\frac{\mathbf{v_3}\cdot\mathbf{x}}{2} + i\phi_3\right), \tag{4}$$

where the $\mathbf{x_i}$ are the initial positions of the solitons, $\mathbf{v_i}$ their initial velocities and ϕ_i their initial phases. Boldface symbols are two-dimensional vectors. The $f_i(.)$ are the soliton profiles, where f_1 is a flat-top soliton, corresponding to the liquid where the dynamics takes place and f_2, f_3 are smaller solitons that dynamically generate the dark excitations. In Fig. 1, we plot the profiles of the particular solitons that will be used in all the examples below.

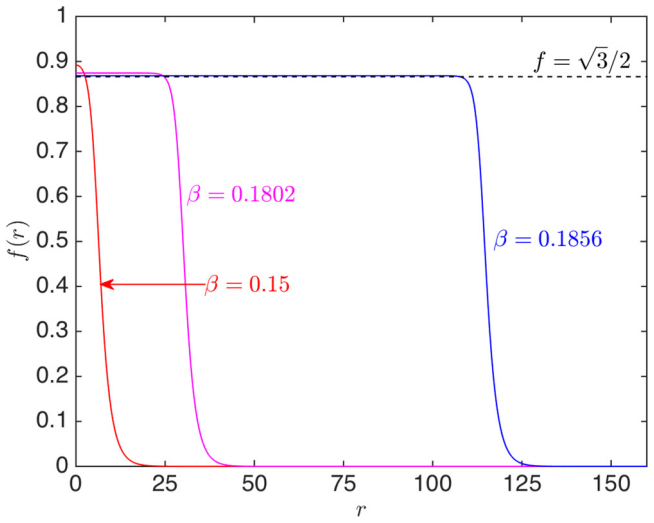

FIG. 1. Radial profiles of the three solitons used to define the initial conditions in the examples below. Their powers $P = 2\pi\int_0^\infty r f(r)^2 dr$ are $P|_{\beta=0.15} = 86.0$, $P|_{\beta=0.1802} = 2055.5$, $P|_{\beta=0.1856} = 30620$.

Let us now turn to the dark traveling waves [30]. They are form-preserving solutions of Eq. (3) moving at constant speed U in, say, the x direction, embedded in an infinite liquid. Inserting the ansatz $\psi(x, y, z) = e^{i\beta_{cr} z}\Psi(\eta, y)$ [32], where $\eta = x - Uz$, we can write:

$$iU\partial_\eta \Psi = \left(\partial_\eta^2 + \partial_y^2\right)\Psi + \left(|\Psi|^2 - |\Psi|^4 - \tfrac{3}{16}\right)\Psi \tag{5}$$

subject to the boundary condition $\lim_{\eta^2+y^2\to\infty} \Psi = \Psi_{cr} = \frac{\sqrt{3}}{2}$. There is a family of solutions parameterized by $0 < U < \frac{\sqrt{3}}{2}$. For small U they are vortex-antivortex pairs, with $|\psi|^2 = 0$ at the phase singularities. When U grows, the vortex and antivortex merge into a rarefaction pulse, whose $|\psi|^2$ is nowhere vanishing. It is important to remark that the transition is completely smooth and, roughly, one can think of the rarefaction pulse as a bound state of vortex and antivortex. In fact, under nontrivial dynamical evolution both kinds of eigenstates can transform into each other [45,47].

An interesting quantity is the current density, which, in the hydrodynamical picture, represents the flow of the fluid.

$$\mathbf{j} = \frac{1}{i}(\psi^*\nabla\psi - \psi\nabla\psi^*). \tag{6}$$

The $\mathbf{j}$ is essential to understand how the dark excitation modifies the medium around it and therefore to understand the interaction between traveling waves. In Fig. 2, we depict this quantity for three examples of traveling waves.

Momentum and energy are conserved quantities defined by

$$p = \frac{1}{2i}\int [(\Psi^* - \Psi_{cr})\partial_x\Psi - (\Psi - \Psi_{cr})\partial_x\Psi^*] dx dy$$
$$E = \int |\nabla\Psi|^2 dx dy + \frac{1}{3}\int |\Psi|^2\left(|\Psi|^2 - \Psi_{cr}^2\right)^2 dx dy. \tag{7}$$

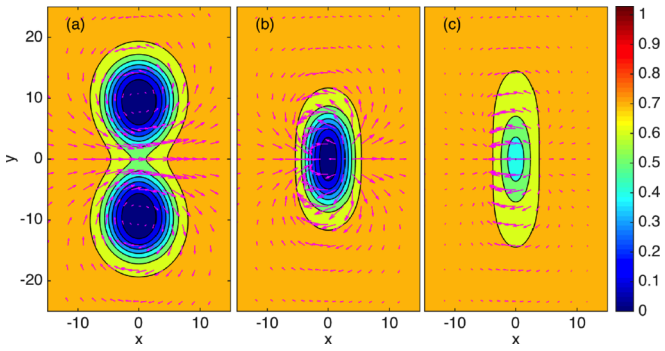

FIG. 2. Three numerically computed traveling waves with $U = 0.11$ [vortex-antivortex pair, (a)], $U = 0.35$ [rarefaction pulse, (b)], and $U = 0.71$ [faint rarefaction pulse, (c)]. The dark excitations are moving rightwards. The color scale displays the density $|\psi|^2$ and the arrows represent the current density $\mathbf{j}$.

Within the family of solutions, one can check that $U = \partial E/\partial p$ and three virial identities are satisfied [30,32,33].

The analysis in the coming sections results from the numerical integration of Eq. (3) with initial conditions (4). The computations are done using a standard split-step beam propagation method [51]. The evolution associated to the nonderivative terms is computed with a fourth-order Runge-Kutta method. The plotted figures are built using grids of 800×600 points. We have checked convergence of the method by comparing results with different grids in (x,y) and steps in z.

III. COHERENT GENERATION OF VORTEX-ANTIVORTEX PAIRS

In Ref. [30], it was shown that a rarefaction pulse can appear when two coherent bright solitons meet with appropriate relative velocity and phase. Roughly speaking, destructive interference generates a void at the collision point, which can acquire the necessary velocity thanks to the incoming momentum. Although, definitely, an exact solution of (5) is not realized in the dynamical process, the resulting robust dark excitation can indeed be identified with a traveling wave solution. This fact was checked in Ref. [30] by comparing the dispersion relations. Even if the size of the medium (the large soliton) is not infinite, it can support the traveling wave if it is much larger than the dark structure.

In this section, we show that a similar process can result in the formation of a vortex-antivortex pair. In fact, the difference with Ref. [30] is simply that the incoming soliton has to be larger. What happens is that during a collision in phase opposition, an elongated dark region is created. It cannot be stable because there are no rarefaction pulse solutions of similar size. Consequently, it evolves and decays through a snake instability giving rise to the separate vortex and antivortex, which move forward together with a given velocity U. Since the resulting configuration is not exactly equal to the stationary solution, the dark regions can change, reconnect, and split again. However the vortex-antivortex profile becomes apparent after long enough propagation in z. An example is depicted in Fig. 3. Obviously, the third soliton of (4) is not included in the initial condition.

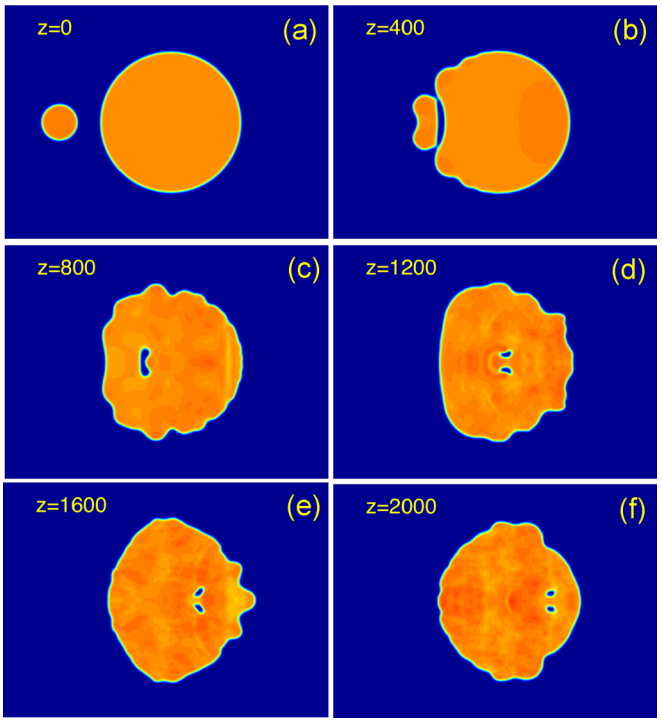

FIG. 3. The encounter of two bright solitons giving rise to a traveling vortex-antivortex pair. Initial conditions have $\mathbf{x_2} = (-180,0)$, $\mathbf{v_2} = (0.2,0)$, $\phi_2 = 5$. The large soliton is the one with $\beta_1 = 0.1856$ and the smaller one has $\beta_2 = 0.1802$. The color code for $|\psi|^2$ is as in Fig. 2 and the range of the axes is $x \in [-270,270]$, $y \in [-190,190]$. An animation is provided in the Supplemental Material [48].

In Fig. 4, we expose the phase structure of the wave function of the example at a particular propagation distance z. The plots prove that the two dark spots of Fig. 3 correspond indeed to a vortex-antivortex pair.

Concerning the reconversion into a bright soliton [30], we notice that it can take place when the excitation reaches the boundary of the liquid of light as a single dark pulse. On the

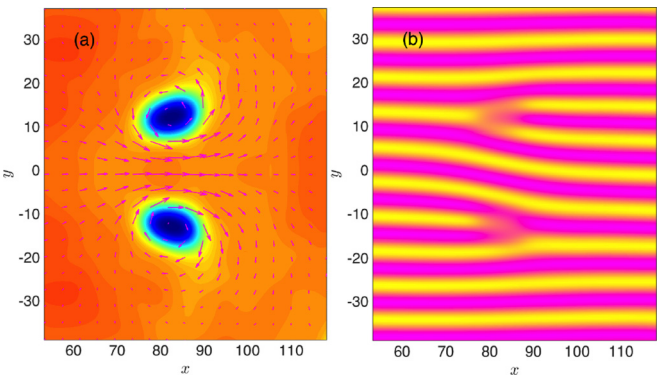

FIG. 4. Phase structure of the wave function. The plot corresponds to $z = 2000$, Fig. 3(f). The region of the vortex-antivortex has been enlarged. (a) depicts $|\psi|^2$ with the same color scale of Fig. 2 and the arrows are a quiver diagram for $\mathbf{j}$ showing flows similar to Fig. 2. (b) corresponds to the interference pattern with a plane wave: $|\psi(x,y,z = 2000) + 7\exp(-100iy)|^2$. The forklike structures prove the existence of a vortex-antivortex pair with charges ±1.

other hand, when it does so as a vortex-antivortex pair, two waves propagating in opposite directions along the edge of the large soliton get excited [48].

It must be emphasized that the generation of vortex and antivortex is only one of the possible qualitative outcomes that emerge depending on the relative velocity and phase. As in Ref. [30], the droplets can simply coalesce into one. The collision can also result in rarefaction pulses of different energies and speeds. For low velocities, part of the energy can bounce back evolving into a smaller bright soliton. In all cases, surface and bulk sound waves are excited during the process. If the collision is very violent, the large soliton can be severely distorted, ceasing to be a liquidlike approximately homogeneous medium.

We close this section by noting that there are vortex solutions of the cubic-quintic equation (3) of the form $\psi = e^{i\beta z}e^{il\theta}f(r)$ with $\lim_{r\to\infty} f(r) = 0$, where l is the topological charge and θ is the polar angle. Their profiles and stability have been studied in Refs. [52–56] and their collisional dynamics in Ref. [57]. We remark that the vortices that we are studying in this paper as solutions of Eq. (5) are different objects: they live within the vorticityless liquid of light and they only exist in pairs and moving with a finite velocity.

IV. COLLISIONS OF VORTEX-ANTIVORTEX PAIRS

Let us start illustrating the interactions by computing the head-on encounter of two vortex pairs created as described in Sec. III. A typical example is displayed in Fig. 5. The result is an exchange in which the vortex of each pair recombines with the antivortex of the other one (the exchange of a single vortex with a vortex-antivortex pair was described in Ref. [47] with cubic nonlinear potential.) The solitary waves come out perpendicular to the incoming direction. This can be understood in terms of the flow lines of Eq. (6), considering that, during the approach, each pair generates a smooth inhomogeneity in the background in which the other one propagates [46]. For instance, the antivortex on the top right [see Figs. 5(c) and 5(d)] is affected by the flow lines generated by the phase structure of the vortex on the top left (see Fig. 4) and is pushed upwards. Conversely, the vortex in the bottom right turns downwards because of the antivortex in the bottom left. Since these bends tend to associate again vortex and antivortex, the propagation can continue after the exchange. In Fig. 5, we have considered slightly different phases for the initial solitons in order to show that a perfect symmetry is not needed for this process.

Similar exchanges can happen for collisions at angles. Figure 6 depicts an example where the incoming excitations are perpendicular to each other. In this case, the vortex moving downwards and the antivortex moving leftwards attract each other and coalesce into a dark blob, which can be considered an excited version of a rarefaction pulse. It comes out heading towards the top right of the plot and is finally reconverted into a (highly excited) bright soliton when it reaches the edge of the medium. The remaining vortex and antivortex eventually couple to each other and continue to propagate towards the bottom left. Notice that the velocity of this pair is much lower than that of the aforementioned rarefaction pulse, as expected from the stationary solutions characterized in Sec. II.

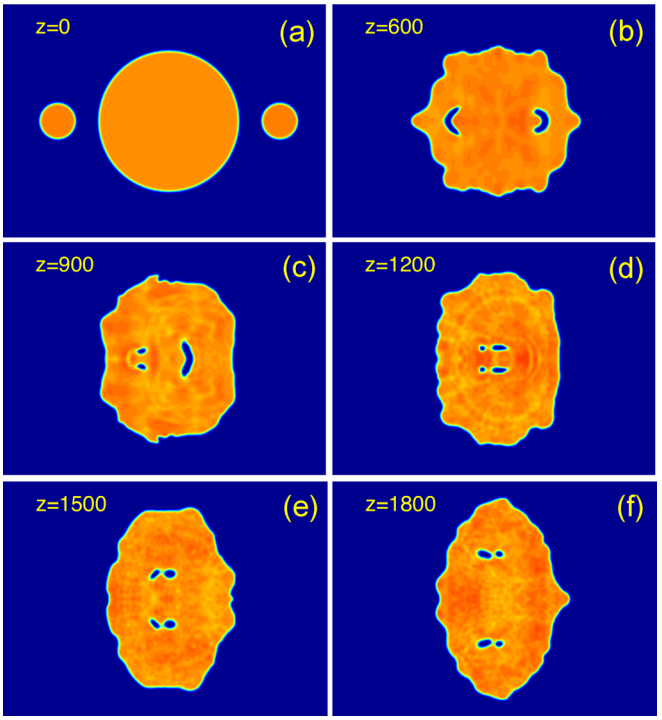

FIG. 5. Head-on encounter of two vortex-antivortex pairs resulting in an exchange mode. Initial conditions are defined by Eq. (4) with $-\mathbf{x_2} = \mathbf{x_3} = (180,0)$, $\mathbf{v_2} = -\mathbf{v_3} = (0.2,0)$, $\phi_2 = 5.3$, $\phi_3 = 5$. The large soliton is the one with $\beta_1 = 0.1856$ and the smaller ones have $\beta_2 = \beta_3 = 0.1802$. Color code and axes are defined as in Fig. 3. An animation is provided in the Supplemental Material [48].

The simulation of Fig. 6 is also interesting because it shows other generic features of the dynamics, which can be better appreciated in the animation presented in the Supplemental Material [48]. In particular, we must emphasize that the evolution of the dark excitations is not elastic, in the sense that some energy is radiated away in the form of sound waves. Moreover, faint rarefaction pulses of small energy, regarding Eq. (7), can be generated. These radiation processes take place during collisions and also during the relaxation of the coherently generated dark bubbles towards their stationary vortex pair form.

We also remark that, for encounters like that of Fig. 6, small changes in the initial conditions can determine how the dark regions combine and greatly affect the out-coming pulses. For instance, if we just change $\mathbf{v_3}$ from $(-0.2,0)$ to $(-0.21,0)$, therefore breaking the symmetry between both incoming vortex pairs, the one moving horizontally arrives first. Instead of performing an exchange with the other vortex, it merges with the antivortex, creating an elongated void of net vorticity -1. This snakelike structure starts rotating and eventually decays emitting a rarefaction pulse. We present this evolution in the Supplemental Material [48]. Thus, the encounter gives rise to a vortex-antivortex pair and a rarefaction pulse, just as in Fig. 6, but their resulting propagation directions are rather different. This simulation also shows that, when there is an eventual dark-bright reconversion, the outgoing dark soliton does not necessarily come out with the same propagation direction as the dark blob that generates it.

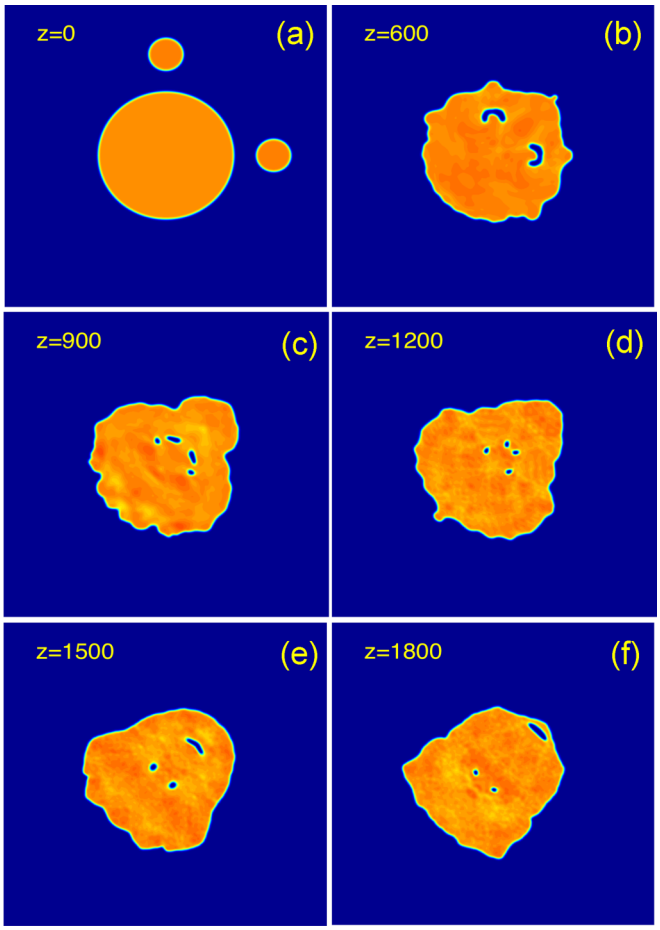

FIG. 6. Encounter at a right angle of two vortex-antivortex pairs resulting in an exchange mode. Initial conditions are defined by Eq. (4) with $\mathbf{x_2} = (0,180)$, $\mathbf{x_3} = (180,0)$, $\mathbf{v_2} = (0,-0.2)$, $\mathbf{v_3} = (-0.2,0)$, $\phi_2 = \phi_3 = 5$. The large soliton is the one with $\beta_1 = 0.1856$ and the smaller ones have $\beta_2 = \beta_3 = 0.1802$. The color code is defined as in Fig. 2. The range of the axes is $x,y \in [-270,270]$. An animation is provided in the Supplemental Material [48].

We close this section by considering a head-on encounter in which the vortices of each pair meet each other (instead of heading an antivortex as in Fig. 5). This can be accomplished by slightly shifting the y position of the bright solitons defined in the initial conditions. An example is depicted in Fig. 7.

This evolution can be qualitatively understood noting that the vortices repel each other and therefore are slowed down while the antivortices continue advancing. This induces a rotation of the whole dark structure, which eventually breaks down resulting in two separate pulses, which come out at an angle, different from the incoming one. This is a kind of pseudoelastic collision. Notice, however, that the scattered pulses cannot be neatly considered vortex-antivortex as the incoming ones. Vortex pairs and rarefaction pulses can be cleanly defined for stationary situations but in dynamical evolutions like the present one, the separation between both is not obvious and they can even transform into each other, as noticed in Ref. [47] in a different but somewhat related scenario.

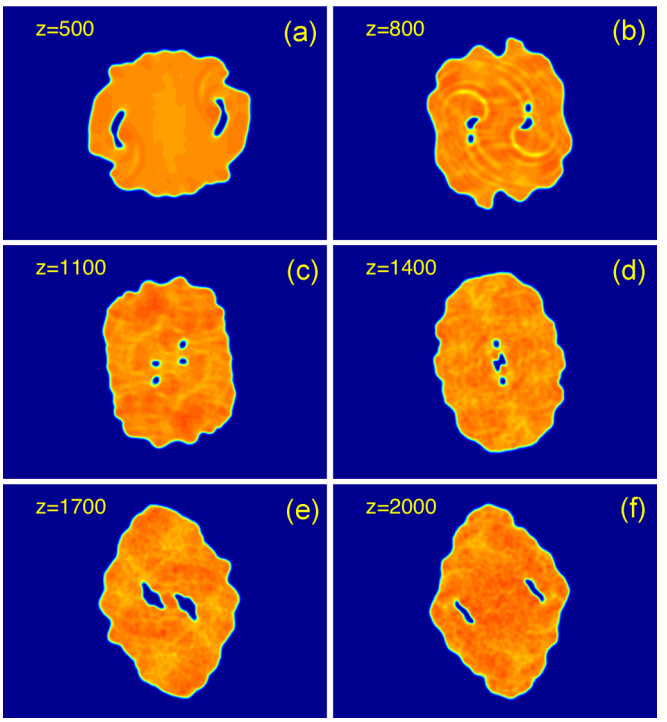

FIG. 7. Encounter of two vortex-antivortex pairs, shifted with respect to each other along the direction transverse to propagation, resulting in pseudoelastic scattering. Initial conditions are defined by Eq. (4) with $\mathbf{x_2} = (-180,-10)$, $\mathbf{x_3} = (180,10)$, $\mathbf{v_2} = (0.2,0)$, $\mathbf{v_3} = (-0.2,0)$, $\phi_2 = \phi_3 = 5$. The large soliton is the one with $\beta_1 = 0.1856$ and the smaller ones have $\beta_2 = \beta_3 = 0.1802$. Color code and axes range are defined as in Fig. 3. An animation is provided in the Supplemental Material [48].

V. COLLISION OF A RAREFACTION PULSE WITH A VORTEX-ANTIVORTEX PAIR

We now consider the encounter of a rarefaction pulse with a vortex-antivortex pair. An illustrative case is sketched in Fig. 8. In the example, the dark regions moving in opposite directions pass near each other but do not experience a direct contact. They keep their distinct identities during the whole evolution and therefore this process is very similar to a elastic scattering. The pulses continue their propagation away from each other and therefore we call this a flyby mode, following Ref. [47]. In the figure, it can be appreciated that the propagation of the rarefaction pulse is rotated by a small angle when both waves meet (the horizontal dashed line has been included in the plots to guide the eye). Again, this is due to the flow lines defined in Eq. (6) and represented in Fig. 2, whose structure explains why the caviton turns upwards. The vortex-antivortex pair is also affected by the encounter, by since its energy and momentum (7) is quite larger that that of the rarefaction pulse, it is much harder to appreciate the diversion. Notice that this flyby mode is only relevant for a narrow window of the scattering impact parameter. If the caviton pulse moves far from the dipolar structure, the phase gradients are tiny and their effect is negligible. On the other hand, if both waves are too near, the dark regions recombine giving rise to more complicated evolutions, as we show in the next example.

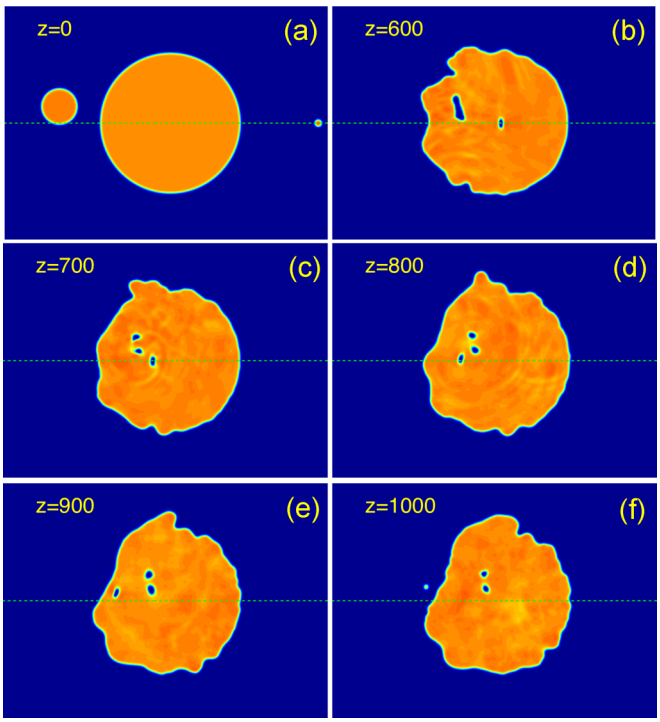

FIG. 8. Flyby encounter of a rarefaction pulse with a vortex-antivortex pair. The pulse trajectory is modified because of the flows generated by the vortex-antivortex phase structure. The horizontal dashed line marks $y = 0$, the path that the rarefaction pulse would follow in the absence of other excitations. Initial conditions are defined by Eq. (4) with $\mathbf{x_2} = (-180,27)$, $\mathbf{x_3} = (240,0)$, $\mathbf{v_2} = (0.2,0)$, $\mathbf{v_3} = (-0.5,0)$, $\phi_2 = 4.9$, $\phi_3 = 4$. The large soliton is the one with $\beta_1 = 0.1856$ and the smaller ones have $\beta_2 = 0.1802$ and $\beta_3 = 0.15$. Color code and axes range are defined as in Fig. 3. An animation is provided in the Supplemental Material [48].

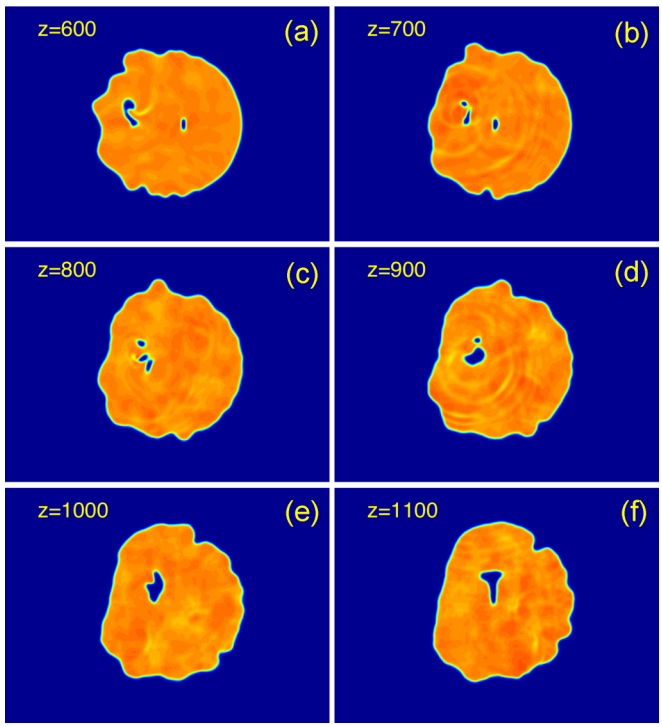

FIG. 9. Inelastic collision of a rarefaction pulse and a vortex-antivortex pair. The rarefaction pulse touches the antivortex, blends with it and, eventually, also gets connected to the dark region around the vortex. The resulting structure can be considered as a highly excited vortex-antivortex pair which continues to propagate within the liquid of light. Initial conditions are defined by Eq. (4) with $\mathbf{x_2} = (-180,18)$, $\mathbf{x_3} = (240,0)$, $\mathbf{v_2} = (0.2,0)$, $\mathbf{v_3} = (-0.5,0)$, $\phi_2 = 4.9$, $\phi_3 = 5$. The large soliton is the one with $\beta_1 = 0.1856$ and the smaller ones have $\beta_2 = 0.1802$ and $\beta_3 = 0.15$. Color code and axes range are defined as in Fig. 3. An animation is provided in the Supplemental Material [48].

The initial conditions in Fig. 9 resemble those of Fig. 8, but the initial y displacement of the bright solitons is slightly smaller, yielding a smaller impact parameter for the collision of the dark waves. In this case, the dark regions associated to the antivortex and the rarefaction pulse come into contact and merge, initially giving rise to a large blob of vorticity -1. Since the vortex-antivortex pair has the larger momentum and energy, the subsequent evolution can be roughly described as an absorption of the rarefaction pulse by the pair, which becomes highly excited, but continues its propagation rightwards. This structure slowly relaxes towards the stationary vortex-antivortex solution by the emission of sound waves and faint rarefaction pulses [48]. In the Supplemental Material [48], we also present a simulation in which the vortex pair and the caviton approach each other with zero impact parameter. Roughly, the dynamics can be understood in terms of the previous discussion: when the dark regions touch each other, the rarefaction pulse is swallowed by the vortex-antivortex, which, albeit excited, continues its propagation. We have checked that this kind of qualitative behavior is quite generic, regardless of the incoming angles and velocities.

VI. COLLISIONS OF RAREFACTION PULSES

Let us now discuss the case of two interacting rarefaction pulses. First of all, we notice the existence of flyby modes, similar to those described in the previous section, when the impact parameter is not too large but enough to avoid direct contact.

It is also worth commenting on the dynamics of head-on collisions. The most common result is illustrated in Fig. 10. When the pulses meet, a larger dark blob is created with, possibly, a bright spot inside [see Fig. 10(d)]. Then, two rarefaction pulses appear again and continue their propagation. During the encounter, part of the energy is radiated away and, therefore, the pulses after the collision are slightly fainter and faster. Thus, in this respect, the rarefaction pulses behave as dark quasisolitons. We remark that this happens for symmetric encounters as the one of the figure or asymmetric ones with pulses of different energies. As expected, when the cavitons reach the edge of the large soliton, they can be reconverted in bright solitons again. In fact, the simulation of Fig. 10 can be interpreted as a bright-dark-bright-dark-bright transformation of the propagating excitation [48].

Curiously, the picture changes completely if the initial conditions are properly fine tuned. Figure 11 depicts an example in which the rarefaction pulses annihilate each other and their energy is radiated in the form of a circular sound wave. Visibly, the behavior of the rarefaction pulses in this

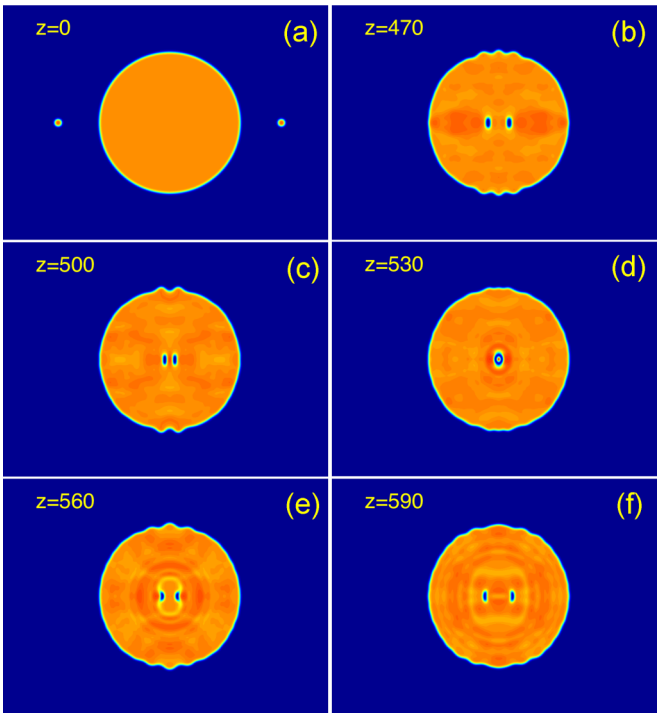

FIG. 10. Symmetric head-on encounter of two rarefaction pulses, which cross each other, losing a fraction of their energy in the process. Initial conditions are defined by Eq. (4) with $-\mathbf{x_2} = \mathbf{x_3} = (180,0)$, $\mathbf{v_2} = -\mathbf{v_3} = (0.5,0)$, $\phi_2 = \phi_3 = 6$. The large soliton is the one with $\beta_1 = 0.1856$ and the smaller ones have $\beta_2 = \beta_3 = 0.15$. Color code and axes range are defined as in Fig. 3. An animation is provided in the Supplemental Material [48].

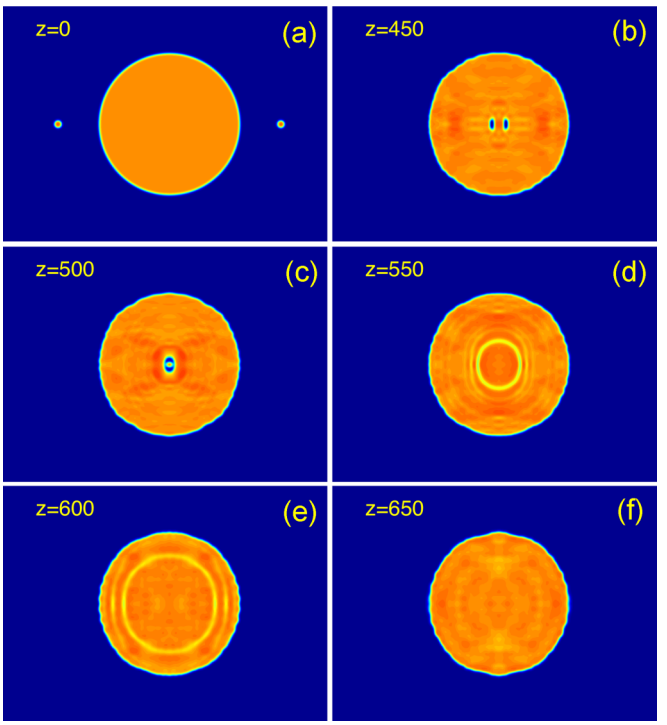

FIG. 11. Symmetric head-on encounter of two rarefaction pulses resulting in a fully inelastic collision. The pulses annihilate each other and yield all their energy to a circular sound wave. Initial conditions are defined by Eq. (4) with $-\mathbf{x_2} = \mathbf{x_3} = (180,0)$, $\mathbf{v_2} = -\mathbf{v_3} = (0.5,0)$, $\phi_2 = \phi_3 = 4.8$. The large soliton is the one with $\beta_1 = 0.1856$ and the smaller ones have $\beta_2 = \beta_3 = 0.15$. Color code and axes range are defined as in Fig. 3. An animation is provided in the Supplemental Material [48].

case totally differs from that of form preserving solitons. As a matter of fact, the seemingly antagonistic character of Figs. 10 and 11 can be continuously connected by noticing that in all head-on encounters the outgoing energy is shared by a bulk wave and two rarefaction pulses. In Fig. 10, most of the energy goes to the latter whereas in Fig. 11 it is mostly acquired by the former, while other initial conditions lead to intermediate possibilities.

Finally, we comment on the encounter of rarefaction pulses at angles. Figure 12 illustrates this case by considering a perpendicular concurrence. As in the previous cases, the dark regions combine producing a dark blob, which is larger than the incoming ones. However, in this case this blob can survive and, in a loose sense, propagate in the direction required by momentum conservation. Thus, the simulation of Fig. 12 can be neatly portrayed as the merging of two rarefaction pulses into a more energetic one. Similarly to all of the presented examples, part of the energy is radiated away during the process.

We close the section by noticing that there is a second typical qualitative behavior, which we show in the Supplemental Material [48]. What happens there is that the dark blob splits giving rise again to two rarefaction pulses (we emphasize that, even if it may seem that the dark pulses coming out of the collision propagate almost in parallel, they are not vortex and antivortex). Roughly, this last possibility can be thought of as another example of quasielastic scattering or as a bounce of the pulses against each other.

VII. SUMMARY AND OUTLOOK

In this work, we have numerically analyzed Eq. (3), reporting on a number of qualitative phenomena for the cubic-quintic model in 1+2 dimensions. The interplay of diffraction with focusing and defocusing nonlinear effects endows the cubic-quintic nonlinear Schrödinger equation with an extremely rich phenomenology. In particular, there are dark traveling waves and bright solitons, which for large powers become liquidlike. Noticeably, the dark and bright stationary and stable solitary waves can transform into each other during evolution. In particular, a bright soliton can excite a rarefaction pulse when it meets a bright soliton of larger power [30]. We have shown that a vortex-antivortex pair can be generated in a similar way. The process, however, is not as clean as in the previous case. The incoming soliton has to be larger and gives rise to a more pronounced distortion of the flat-top soliton. Moreover, the vortex and antivortex are not generated directly, but only as the end result of a snake instability of an initial dark blob. Thus, the radiation of part of the excess energy is essential in approaching the stationary vortex-antivortex solution. When a strong enough rarefaction pulse reaches the border of the liquid of light, it typically generates an outgoing bright soliton. On the other hand, the vortex-antivortex pair excites a couple of surface waves propagating in opposite directions.

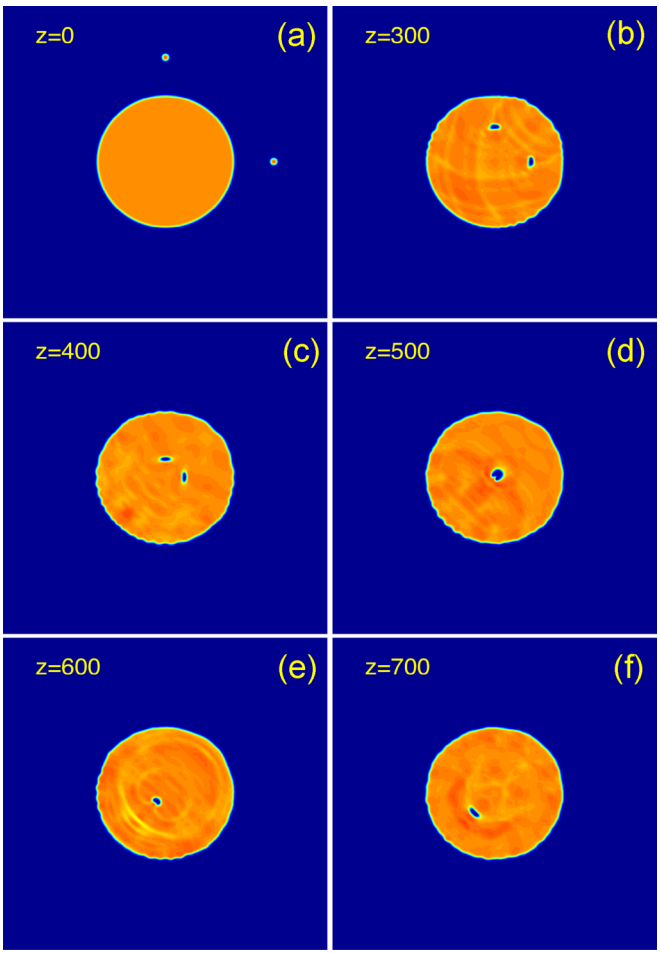

FIG. 12. Two rarefaction pulses collide perpendicularly and merge. Initial conditions are defined by Eq. (4) with $\mathbf{x_2} = (0,180)$, $\mathbf{x_3} = (180,0)$, $\mathbf{v_2} = (0,-0.5)$, $\mathbf{v_3} = (-0.5,0)$, $\phi_2 = \phi_3 = 5$. The large soliton is the one with $\beta_1 = 0.1856$ and the smaller ones have $\beta_2 = \beta_3 = 0.15$. The color code is defined as in Fig. 2. The range of the axes is $x, y \in [-270,270]$. An animation is provided in the Supplemental Material [48].

The possibility of creating the dark states by interference and nonlinear evolution has allowed us to propose numerical experiments concerning their scattering with initial conditions, which only include bright solitons, see Eq. (4). We have made a qualitative analysis of the encounters between vortex-antivortex pairs and rarefaction pulses. In brief, our results can be summarized as follows.

(i) If the vortex of a pair meets an antivortex of another pair and vice versa, they tend to get exchanged resulting in two new pairs with different propagation directions.

(ii) If the impact parameter of a collision is large enough and the dark regions do not touch each other, there are elastic flyby modes and the propagation direction of each wave is altered because of the flow lines associated to the opposite structure.

(iii) When a vortex or a rarefaction pulse touches a vortex-antivortex pair, an excited dark blob is created. It propagates for a while and eventually decays approaching the stationary states. The end result is strongly dependent on initial conditions.

(iv) Rarefaction pulses that collide head-on typically cross each other, losing some energy by radiating sound waves. In particular situations, the radiation can take most of the energy. If the pulses collide at an angle, they can merge into a larger rarefaction pulse or scatter quasielastically.

This list does not exhaust the possibilities but it certainly provides a qualitative description for most of the collisions between dark traveling waves. It is tempting to interpret the traveling waves as quasiparticles and to try to understand collisions in terms of their energy-momentum conservation, Eq. (7). Implicitly, this has been our point of view when using the words "elastic" and "inelastic". Notice that p and E as a whole are conserved in a collision. Nevertheless, if we only take into account the dark traveling waves, the conservation breaks down, as it obvious from Fig. 10. The main reason is that sound waves take a sizable fraction of energy and momentum in many processes. Moreover, as we have already emphasized, the dark waves typically appear in excited form and therefore the velocity-momentum and dispersion relations that can be deduced from the stationary solutions only apply approximately. Excited dark states have complicated dynamics and cannot always be easily identified with their stationary counterparts. Thus, the quasiparticle interpretation is illustrative but it should be clear that it is just a qualitative rough description.

Our results open some interesting possibilities. First of all, it would be nice to realize the described phenomena in optical setups along the lines of Refs. [21–23]. It would also be desirable to study similar effects in two dimensions for the cubic defocusing nonlinearity, since it is relevant for Bose-Einstein experiments such as Ref. [38], see also Ref. [58] and references therein. Moreover, it would be worth considering the three-dimensional cubic-quintic case, which supports flat-top stable spatiotemporal solitons [59,60] and vortices [59,61]. Their collisional dynamics has been analyzed in Refs. [62,63] but the dynamics of dark traveling waves has not been described yet. Using the cubic defocusing Schrödinger equation, interesting dynamical analysis of the interplay of rarefaction pulses, vortex rings and vortex lines in 1+3 dimensions have been presented in the context of Bose-Einstein condensates [64–66] and superfluids [67]. It would be desirable to make contact with these analyses in the cubic-quintic case. Finally, we remark that our setup has partial similarities with other physical systems as, e.g., the scattering by impurities in superfluids as recently modeled in Ref. [68]. It could be worth exploring analogies between different frameworks.

ACKNOWLEDGMENTS

We thank David Nóvoa and José Ramón Salgueiro for useful comments. This work is supported by Grant No. FIS2014-58117-P from Ministerio de Economía y Competitividad and Grants No. GPC2015/019 and No. EM2013/002 from Xunta de Galicia. The work of D.F. is supported by Ministerio de Educacion, Cultura y Deporte (Spain) through the FPU Ph.D. program.

[1] I. B. Burgess, M. Peccianti, G. Assanto, and R. Morandotti, Phys. Rev. Lett. **102**, 203903 (2009).
[2] F. Setzpfandt, D. N. Neshev, R. Schiek, F. Lederer, A. Tünnermann, and T. Pertsch, Opt. Lett. **34**, 3589 (2009).
[3] K.-H. Kuo, Y. Y. Lin, R.-K. Lee, and B. A. Malomed, Phys. Rev. A **83**, 053838 (2011).
[4] U. A. Laudyn, M. Kwasny, A. Piccardi, M. A. Karpierz, R. Dabrowski, O. Chojnowska, A. Alberucci, and G. Assanto, Opt. Lett. **40**, 5235 (2015).
[5] F. Maucher, T. Pohl, S. Skupin, and W. Krolikowski, Phys. Rev. Lett. **116**, 163902 (2016).
[6] D. Novoa, D. Tommasini, and H. Michinel, Europhys. Lett. **98**, 44003 (2012).
[7] D. Mihalache, M. Bertolotti, C. Sibilia, and D. Mazilu, J. Opt. Soc. Am. B **5**, 565 (1988).
[8] D. Pushkarov and S. Tanev, Opt. Commum. **124**, 354 (1996).
[9] K. Dimitrevski, E. Reimhult, E. Svensson, A. Öhgren, D. Anderson, A. Berntson, M. Lisak, and M. L. Quiroga-Teixeiro, Phys. Lett. A **248**, 369 (1998).
[10] H. Michinel, J. Campo-Táboas, R. García-Fernández, J. R. Salgueiro, and M. L. Quiroga-Teixeiro, Phys. Rev. E **65**, 066604 (2002).
[11] C. Josserand and S. Rica, Phys. Rev. Lett. **78**, 1215 (1997).
[12] A. Muryshev, G. V. Shlyapnikov, W. Ertmer, K. Sengstock, and M. Lewenstein, Phys. Rev. Lett. **89**, 110401 (2002).
[13] L. Khaykovich and B. A. Malomed, Phys. Rev. A **74**, 023607 (2006).
[14] R. Carretero-González, D. Frantzeskakis, and P. Kevrekidis, Nonlinearity **21**, R139 (2008).
[15] T. A. Davydova, A. I. Yakimenko, and Y. A. Zaliznyak, Phys. Rev. E **67**, 026402 (2003).
[16] F. Smektala, C. Quemard, V. Couderc, and A. Barthélémy, J. Non-Cryst. Solids, **274**, 232 (2000).
[17] R. M. Caplan, R. Carretero-González, P. G. Kevrekidis, and B. A. Malomed, Math. Comput. Simulat. **82**, 1150 (2012).
[18] A. Piekara, J. Moore, and M. Feld, Phys. Rev. A **9**, 1403 (1974).
[19] M. Centurion, Y. Pu, M. Tsang, and D. Psaltis, Phys. Rev. A **71**, 063811 (2005).
[20] D. Novoa, H. Michinel, D. Tommasini, and A. V. Carpentier, Phys. Rev. A **81**, 043842 (2010).
[21] E. L. Falcao-Filho, C. B. de Araújo, G. Boudebs, H. Leblond, and V. Skarka, Phys. Rev. Lett. **110**, 013901 (2013).
[22] Z. Wu, Y. Zhang, C. Yuan, F. Wen, H. Zheng, Y. Zhang, and M. Xiao, Phys. Rev. A **88**, 063828 (2013).
[23] Z. Wu, Y. Zhang, Z. Ullah, T. Jiang, and C. Yuan, Opt. Express **23**, 8430 (2015).
[24] H. Michinel, M. J. Paz-Alonso, and V. M. Pérez-García, Phys. Rev. Lett. **96**, 023903 (2006).
[25] A. Alexandrescu, H. Michinel, and V. M. Pérez-García, Phys. Rev. A **79**, 013833 (2009).
[26] Z. Bai and G. Huang, Opt. Express **24**, 4442 (2016).
[27] Y. Peng, A. Yang, B. Chen, Y. Xu, and X. Hu, J. Opt. Soc. Am. B **31**, 2188 (2014).
[28] S.-C. Tian, R.-G. Wan, C.-Z. Tong, and Y.-Q. Ning, AIP Adv. **5**, 027111 (2015).
[29] A. S. Reyna and C. B. de Araújo, Opt. Lett. **41**, 191 (2016).
[30] Á. Paredes, D. Feijoo, and H. Michinel, Phys. Rev. Lett. **112**, 173901 (2014).
[31] D. Chiron and C. Scheid, J. Nonlinear Sci. **26**, 171 (2016).
[32] C. Jones and P. Roberts, J. Phys. A **15**, 2599 (1982).
[33] C. Jones, S. Putterman, and P. Roberts, J. Phys. A **19**, 2991 (1986).
[34] N. G. Berloff and P. H. Roberts, J. Phys. A **37**, 11333 (2004).
[35] F. Béthuel, P. Gravejat, and J.-C. Saut, Commun. Math. Phys. **285**, 567 (2009).
[36] I. Barashenkov and V. Makhankov, Phys. Lett. A **128**, 52 (1988).
[37] I. Barashenkov, A. Gocheva, V. Makhankov, and I. Puzynin, Physica D (Amsterdam) **34**, 240 (1989).
[38] H. Proud, M. Perea-Ortiz, C. O'Neale, M. Baumert, M. Holynski, J. Kronjäger, G. Barontini, K. Bongs, and N. Meyer, arXiv:1609.08504.
[39] C. Josserand, Y. Pomeau, and S. Rica, Phys. Rev. Lett. **75**, 3150 (1995).
[40] D. Feijoo, I. Ordónez, A. Paredes, and H. Michinel, Phys. Rev. E **90**, 033204 (2014).
[41] V. A. Mironov, A. Smirnov, and L. A. Smirnov, J. Exp. Theor. Phys. **110**, 877 (2010).
[42] W.-S. Kim and H.-T. Moon, Phys. Lett. A **266**, 364 (2000).
[43] J. Garralón, F. Rus, and F. R. Villatoro, Commun. Nonlinear Sci. Numer. Simulat. **18**, 1576 (2013).
[44] L. A. Smirnov and V. A. Mironov, Phys. Rev. A **85**, 053620 (2012).
[45] V. Mironov and L. A. Smirnov, JETP Lett. **95**, 549 (2012).
[46] V. Mironov and L. Smirnov, Phys. Wave Phen. **21**, 62 (2013).
[47] L. A. Smirnov and A. I. Smirnov, Phys. Rev. A **92**, 013636 (2015).
[48] See Supplemental Material at http://link.aps.org/supplemental/10.1103/PhysRevE.95.032208 for animations of the simulations of Figs. 3, 5–12, and the three extra examples mentioned in the text.
[49] V. Prytula, V. Vekslerchik, and V. M. Pérez-García, Phys. Rev. E **78**, 027601 (2008).
[50] D. Novoa, H. Michinel, and D. Tommasini, Phys. Rev. Lett. **103**, 023903 (2009).
[51] G. P. Agrawal, *Nonlinear Fiber Optics* (Academic Press, New York, 2007).
[52] M. Quiroga-Teixeiro and H. Michinel, J. Opt. Soc. Am. B **14**, 2004 (1997).
[53] I. Towers, A. V. Buryak, R. A. Sammut, B. A. Malomed, L.-C. Crasovan, and D. Mihalache, Phys. Lett. A **288**, 292 (2001).
[54] V. I. Berezhiani, V. Skarka, and N. B. Aleksić, Phys. Rev. E **64**, 057601 (2001).
[55] B. A. Malomed, L.-C. Crasovan, and D. Mihalache, Physica D (Amsterdam) **161**, 187 (2002).
[56] H. Michinel, J. R. Salgueiro, and M. J. Paz-Alonso, Phys. Rev. E **70**, 066605 (2004).
[57] M. J. Paz-Alonso, D. Olivieri, H. Michinel, and J. R. Salgueiro, Phys. Rev. E **69**, 056601 (2004).
[58] G. Verma, U. D. Rapol, and R. Nath, arXiv:1611.06195.
[59] A. Desyatnikov, A. Maimistov, and B. Malomed, Phys. Rev. E **61**, 3107 (2000).
[60] Z. Jovanoski, J. Mod. Opt. **48**, 865 (2001).
[61] D. Mihalache, D. Mazilu, L.-C. Crasovan, I. Towers, A. V. Buryak, B. A. Malomed, L. Torner, J. P. Torres, and F. Lederer, Phys. Rev. Lett. **88**, 073902 (2002).
[62] Y. Hong and T. Yi, Chin. Phys. B **17**, 1008 (2008).

[63] S. K. Adhikari, Phys. Rev. E **94**, 032217 (2016).
[64] N. G. Berloff, Phys. Rev. B **65**, 174518 (2002).
[65] N. G. Berloff, Phys. Rev. A **69**, 053601 (2004).
[66] S. Komineas and J. Brand, Phys. Rev. Lett. **95**, 110401 (2005).
[67] R. Caplan, J. Talley, R. Carretero-González, and P. Kevrekidis, Phys. Fluids **26**, 097101 (2014).
[68] I. A. Pshenichnyuk and N. G. Berloff, Phys. Rev. B **94**, 184505 (2016).